



## Controllable synthesis and characterization of Fe<sub>3</sub>O<sub>4</sub>/Au composite nanoparticles



Yan Xing<sup>a,b</sup>, Yan-Yan Jin<sup>a,b</sup>, Jian-Chao Si<sup>a,b</sup>, Ming-Li Peng<sup>a,b,\*</sup>, Xiao-Fang Wang<sup>a</sup>,  
Chao Chen<sup>b,c</sup>, Ya-Li Cui<sup>b,c,\*\*</sup>

<sup>a</sup> Key Laboratory of Synthetic and Natural Functional Molecular Chemistry of Ministry of Education, College of Chemistry and Materials Science, Northwest University, Xi'an 710069, PR China

<sup>b</sup> National Engineering Research Center for Miniaturized Detection Systems, Xi'an 710069, PR China

<sup>c</sup> College of Life Sciences, Northwest University, Xi'an 710069, PR China

### ARTICLE INFO

#### Article history:

Received 30 July 2014

Received in revised form

29 September 2014

Accepted 29 September 2014

Available online 5 October 2014

#### Keywords:

Fe<sub>3</sub>O<sub>4</sub>/Au composite nanoparticles

Controllable size

Superparamagnetism

### ABSTRACT

Fe<sub>3</sub>O<sub>4</sub>/Au composite nanoparticles (GoldMag NPs) have received considerable attention because of their advantageous properties arisen from both individual Au and Fe<sub>3</sub>O<sub>4</sub> nanoparticles. Many efforts have been devoted to the synthesis of these composite nanoparticles. Herein, GoldMag NPs were reported to be synthesized by two-step method. Fe<sub>3</sub>O<sub>4</sub> nanoparticles were prepared by co-precipitation and modified by the citric acid, and then citric acid-coated Fe<sub>3</sub>O<sub>4</sub> nanoparticles were used as seeds in sodium citrate solution to reduce the HAuCl<sub>4</sub>. The size of obtained nanoparticles was geared from 25 to 300 nm by controlling the concentration of reactants. The GoldMag NPs were characterized by UV–vis spectrometer, dynamic light scattering (DLS), transmission electron microscopy (TEM), X-ray photoelectron spectroscopy (XPS), X-ray diffraction (XRD), and vibrating sample magnetometer (VSM). The GoldMag NPs showed good superparamagnetism at room temperature and were well dispersed in water with surface plasmon resonance absorption peak varied from 538 nm to 570 nm.

© 2014 Elsevier B.V. All rights reserved.

## 1. Introduction

During past few decades, magnetic nanoparticles have aroused remarkable interest in many fields such as biological separation and protein purification [1–3], target delivery [4,5], therapy [6,7], biosensor [8,9] and catalysis [10,11]. GoldMag NPs composed of Fe<sub>3</sub>O<sub>4</sub> and gold nanohybrid material, in particular, have attracted ever-increasing attention due to the noticeable advantages of Au nanoparticles. Gold is an inert element and very useful as a coating material for protecting magnetic nanoparticles, its unique biocompatibility [12], versatility in surface modification [13] and high catalytic properties [14].

The physicochemical property of GoldMag NPs is often dependent upon its particle size and morphology. Many efforts have been made to synthesize GoldMag NPs, such as microemulsion method [15,16], aqueous-phase method [17–19], preparation of oil phase [20–22], phase transfer [23,24]. Recently the preparation of

novel Fe<sub>3</sub>O<sub>4</sub>/Au/Fe<sub>3</sub>O<sub>4</sub> nanoflowers was reported by our group [25]. However, it is still of great interest to devise a low processing cost, simple manipulation and nontoxic method to obtain GoldMag NPs with controllable size and no serious agglomeration.

Herein, a two-step synthetic method was presented. First, Fe<sub>3</sub>O<sub>4</sub> nanoparticles were prepared by co-precipitation and modified by the citric acid. Second, citric acid-coated Fe<sub>3</sub>O<sub>4</sub> nanoparticles were used as seeds in sodium citrate solution to reduce the HAuCl<sub>4</sub> to obtain the GoldMag NPs. The results showed that the size of obtained nanoparticles ranged from 25 to 300 nm by controlling the concentration of reactants.

## 2. Experimental section

### 2.1. Materials and instruments

Ferric chloride (FeCl<sub>3</sub> · 6H<sub>2</sub>O, 99%) and ferrous chloride (FeCl<sub>2</sub> · 4H<sub>2</sub>O, 99%) were obtained from Sigma-Aldrich, USA. HAuCl<sub>4</sub> · 4H<sub>2</sub>O (Au ≥ 47.8%) was product of Shanghai Fine Chemical Research Institute, China. Sodium citrate and citric acid were purchased from Tianjin No. 1 Reagent Factory, China. Ammonium hydroxide was procured from Fuchen Chemical Reagent Factory of Xi'an, China. All chemicals were of analytical grade and used without

\* Corresponding author at: Key Laboratory of Synthetic and Natural Functional Molecular Chemistry of Ministry of Education, College of Chemistry and Materials Science, Northwest University, Xi'an 710069, PR China.

\*\* Corresponding author.

E-mail addresses: [mlpeng@nwu.edu.cn](mailto:mlpeng@nwu.edu.cn) (M.-L. Peng), [yalicui@nwu.edu.cn](mailto:yalicui@nwu.edu.cn) (Y.-L. Cui).

further purification. The ultrapure water ( $\kappa=18.25 \text{ M}\Omega \text{ cm}$ ) was used in our experiments.

Optical properties of nanoparticles were investigated by measuring optical absorption spectra in UV–vis region with a UV-2550 spectrometer. The hydrodynamic diameter was determined by dynamic light scattering (DLS, Malvern Mastersizer 2000). The morphologies of nanoparticles were carried out using a transmission electron microscopy (TEM, H-600). The surface compositions of elements such as Fe and Au in GoldMag NPs were determined by X-ray photoelectron spectroscopy (XPS, K-Alpha). The crystallographic properties of the nanoparticles were recorded on an X-ray diffractometer (XRD, DMAX-2400) with Cu K $\alpha$  radiation. The mass content of Fe and Au in GoldMag NPs was judged from inductively coupled plasma atomic emission spectrometer measurements (ICP-AES, IRIS Advantage). Magnetic properties of the obtained nanoparticles were characterized by vibrating sample magnetometer (VSM, LakeShore 7073).

## 2.2. Synthesis of citric acid-coated Fe<sub>3</sub>O<sub>4</sub> nanoparticles

Fe<sub>3</sub>O<sub>4</sub> magnetic nanoparticles were prepared through co-precipitation of Fe<sup>3+</sup> and Fe<sup>2+</sup> with ammonium hydroxide. Briefly, 2.7 g FeCl<sub>2</sub> · 4H<sub>2</sub>O and 4.0 g FeCl<sub>3</sub> · 6H<sub>2</sub>O were dissolved in 200 mL ultrapure water. Then the mixture was vigorously stirred until the iron salts were completely dissolved. Subsequently, 10 mL ammonia hydroxide was quickly added into the mixture at room temperature. This system was allowed to keep for 15 min at 75 °C under vigorous stirring. After the reaction, the obtained black product was collected on a permanent magnet and washed three times with ultrapure water. To avoid serious agglomeration of Fe<sub>3</sub>O<sub>4</sub> nanoparticles, 150 mL 1.0 wt% citric acid aqueous solution was added into the mixture and stirred for 15 min at 60 °C. The Fe<sub>3</sub>O<sub>4</sub> magnetic nanoparticles modified with citric acid were separated magnetically and washed with ultrapure water three times to remove unreactive impurities. Finally the products were well dispersed in ultrapure water after modification and sonicated for 3–5 min. The whole process was carried out under N<sub>2</sub> protection [26].

## 2.3. Synthesis of GoldMag NPs

A certain amount of sodium citrate solution (pH=9) was brought to boil with vigorous stirring and then the citric acid-coated Fe<sub>3</sub>O<sub>4</sub> nanoparticles were added. After the solution was boiling again, HAuCl<sub>4</sub> solution was immediately added into the flask. The reaction continued and refluxed for some time at 100 °C to allow the thermal reduction of the gold precursor. After the reaction, the GoldMag nanocomposites were precipitated by magnet again, then washed several times and re-dispersed in water and finally stored at 4 °C. The size was controlled by adding the different concentration of reactants with the same ratios. GoldMag NPs with different size exhibited different colors in aqueous solution.

## 3. Results and discussion

### 3.1. Reaction condition optimization

In order to investigate effect of concentration of HAuCl<sub>4</sub> on GoldMag NPs size distribution, a series content of HAuCl<sub>4</sub> (0 mmol/L, 0.59 mmol/L, 1.77 mmol/L, 1.97 mmol/L, 2.16 mmol/L, 2.36 mmol/L and 3.54 mmol/L) was designed in the reaction system, which the excessive amount of sodium citrate and citric acid-coated Fe<sub>3</sub>O<sub>4</sub> nanoparticles was first fixed as 1.825 mL (0.0311 mol/L) and 0.625 mL (20 mg/L), respectively. UV–vis

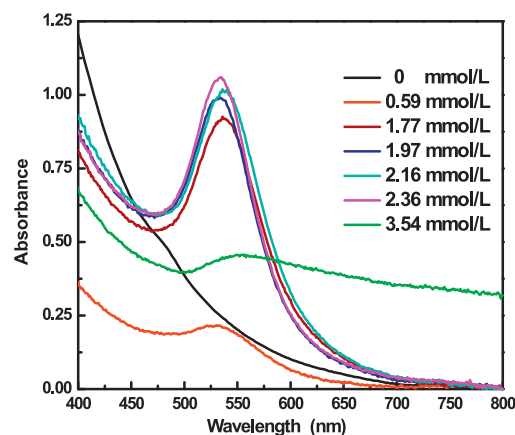


Fig. 1. UV–vis spectra of GoldMag NPs obtained with different concentration of HAuCl<sub>4</sub>.

absorption spectra of GoldMag NPs with different concentration of HAuCl<sub>4</sub> solution are shown in Fig. 1. With the addition of HAuCl<sub>4</sub> solution, the characteristic peaks of surface plasmon resonance appeared and became apparent. As the concentration of HAuCl<sub>4</sub> solution changed from 1.77 to 2.36 mmol/L, the peak was noticeable at around 530–540 nm, which accorded with published data [27]. When the concentration of HAuCl<sub>4</sub> solution increased to

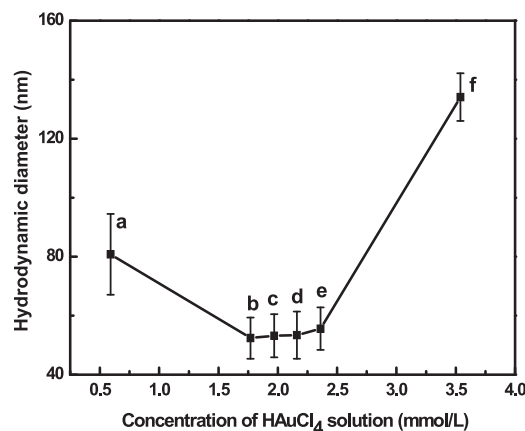


Fig. 2. Hydrodynamic diameter of GoldMag NPs with different concentration of HAuCl<sub>4</sub>: 0.59 mmol/L (a), 1.77 mmol/L (b), 1.97 mmol/L (c), 2.16 mmol/L (d), 2.36 mmol/L (e) and 3.54 mmol/L (f).

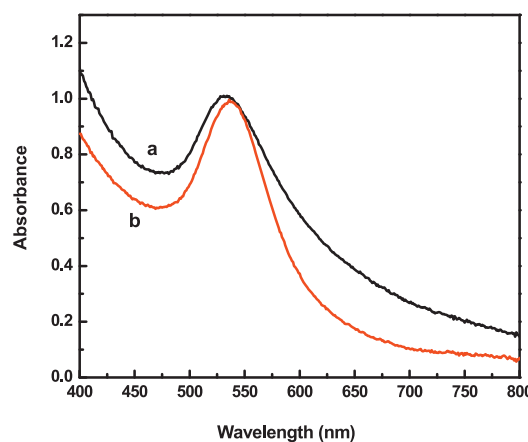


Fig. 3. UV–vis spectra of GoldMag NPs obtained by two different ways: adding HAuCl<sub>4</sub> solution one-time (a) and adding HAuCl<sub>4</sub> solution three-time with an interval of 1 h (b).

3.54 mmol/L, the characteristic absorption peaks broadened, and the color of synthesized GoldMag NPs turned from wine-red to yellow and the corresponding hydrodynamic diameter was found to be larger than 100 nm (Fig. 2f). The hydrodynamic diameter of GoldMag NPs remained basically similar when the concentration of HAuCl<sub>4</sub> solution changed from 1.77 mmol/L to 2.36 mmol/L (Fig. 2b–e). It was not conducive to obtain the desired GoldMag NPs, when the concentration of HAuCl<sub>4</sub> solution was too low or too high (Fig. 2a and f). It was well known from Au nanoparticles preparation that increasing amount of sodium citrate would lead to smaller particle sizes [28]. However, in our experiments, we failed to observe such monotonous phenomenon. This is likely due to the following reasons. Prior to the reaction we fixed the concentration of sodium citrate. When there were not sufficient Au nanoparticles to combine with Fe<sub>3</sub>O<sub>4</sub> nanoparticles, part of

Fe<sub>3</sub>O<sub>4</sub> nanoparticles would lead to aggregation. And when there were too much Au nanoparticles, excess Au nanoparticles also would lead to aggregation. Thus, both cases caused the increasing of the hydrodynamic diameter of GoldMag NPs. This data suggests that the concentration of HAuCl<sub>4</sub> solution play a vital role in hydrodynamic diameter and dispersion of GoldMag NPs in aqueous solution. Considering the economy, the optimum concentration of HAuCl<sub>4</sub> was chosen as 1.77 mmol/L.

Besides the concentration of HAuCl<sub>4</sub>, the times of adding HAuCl<sub>4</sub> solution had also affected the physicochemical property of GoldMag NPs. In this paper, HAuCl<sub>4</sub> solution with fixed amount was added in two different ways: one-time addition and three-time addition with an interval of 1 h. Fig. 3 shows the UV–vis spectra of samples obtained by two ways. The absorption peak of three-time addition (curve b) was sharper and more evident in

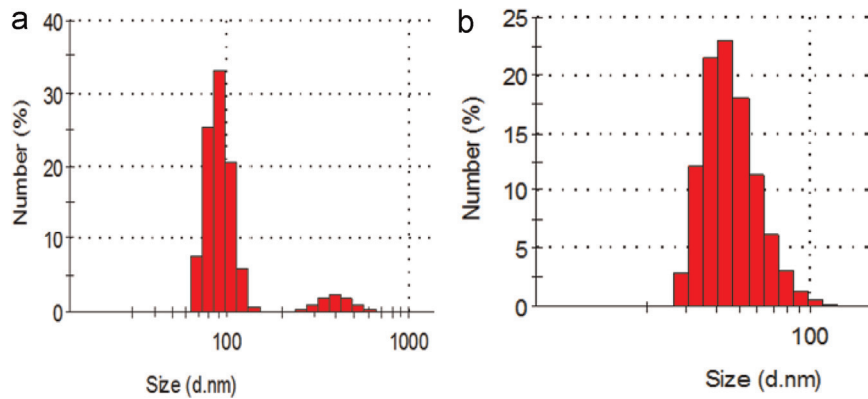


Fig. 4. Size distribution of GoldMag NPs obtained by two different ways: adding HAuCl<sub>4</sub> solution one-time (a) and adding HAuCl<sub>4</sub> solution three-time with an interval of 1 h (b).

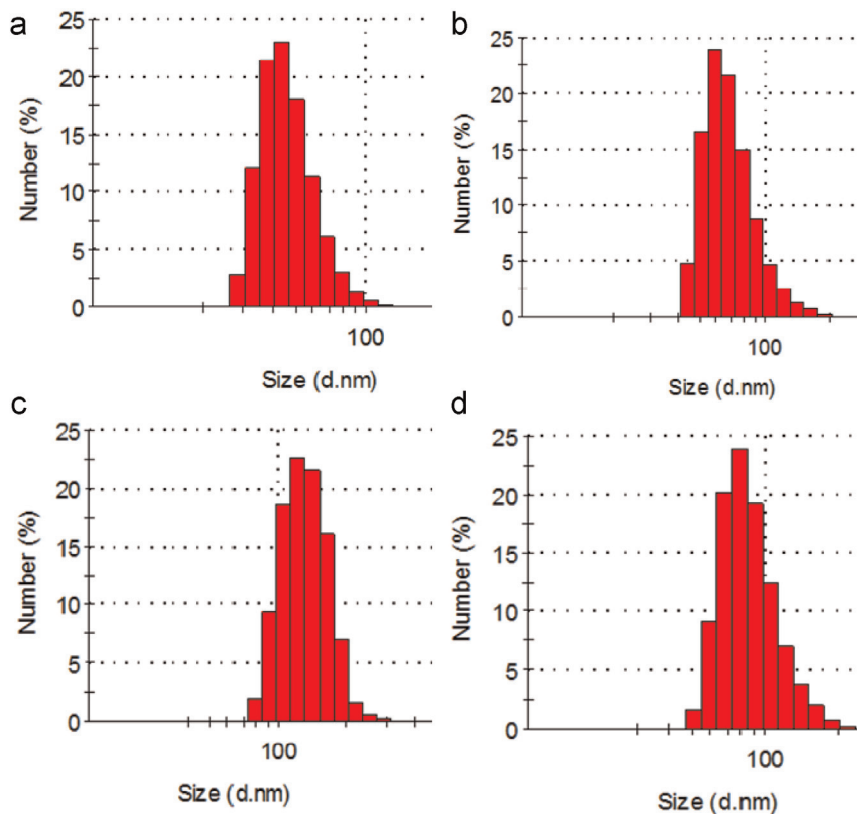
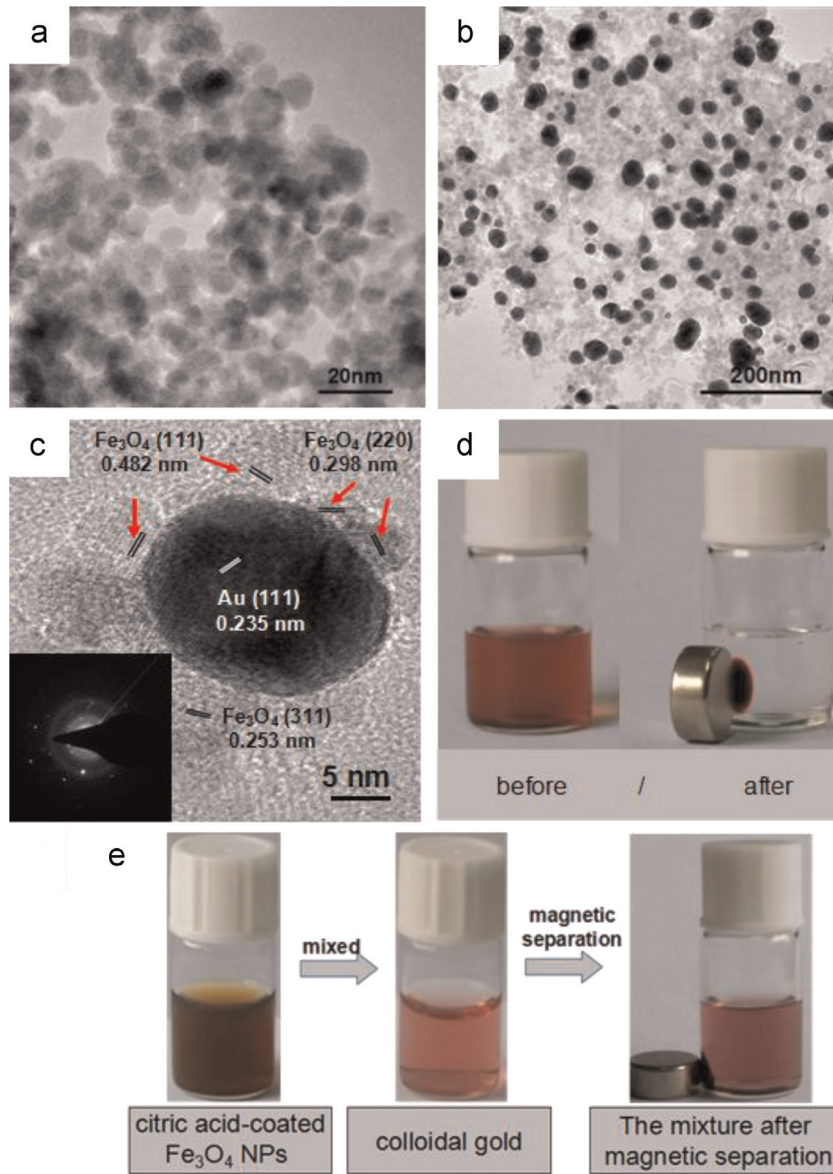
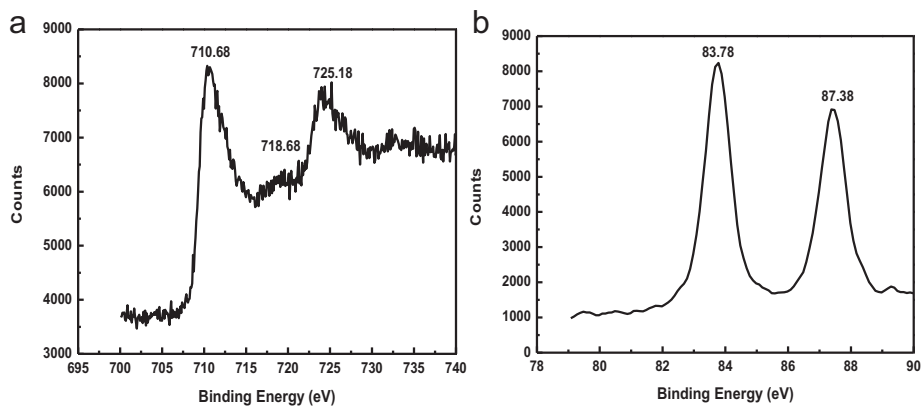


Fig. 5. Size distribution of citric acid-coated Fe<sub>3</sub>O<sub>4</sub> NPs (a) and GoldMag NPs with different aging time of 1 h (b), 3 h(c) and 5 h (d), respectively.



**Fig. 6.** TEM images of citric acid-coated  $\text{Fe}_3\text{O}_4$  (a) and GoldMag NPs (b). The obtained GoldMag NPs was sonicated for 5–10 min and then separated magnetically to discard the supernatant for several times and eventually re-dispersed in water to measure high-resolution TEM (c) and the inset shows the pictures of corresponding selected area electron diffraction (SAED) of synthesized GoldMag NPs. Photograph of magnetic responsiveness of the dilute GoldMag NPs solution (d). Photograph of citric acid-coated  $\text{Fe}_3\text{O}_4$  and colloidal gold solution mixed together and after magnetic separation for 5 min (e).



**Fig. 7.** X-ray photoelectron spectra of Fe (a) and Au (b) of the obtained GoldMag NPs.

comparison with one-time addition (curve a). Furthermore, the size distribution of these two GoldMag NPs shows that the way of one-time addition exhibited a double peak, the size of 92.6% GoldMag NPs was about 91.49 nm, and the size of 7.4% particles was up to 401.5 nm. This data suggests that there is a serious sedimentation as shown in Fig. 4a. Three-time addition had a single peak with average size about 47.20 nm and the width about 14.19 nm as shown in Fig. 4b.

Aging time was also a key element in reaction system. The average diameters of GoldMag NPs with aging 1, 3 and 5 h were 78, 138 and 83 nm (Figs. 5b–d), respectively. This may be arisen from the aging effect that the smaller Au nanolayer would disappear, while the larger Au nanoparticles continued to grow and tended to be uniform as aging time increased. Therefore, 5 h was chosen as the optimum one to synthesize GoldMag NPs.

Consequently, the desired GoldMag NPs synthetic conditions were as follows: adding 1.825 mL (0.0311 mol/L) sodium citrate, 0.625 mL (20 mg/L) citric acid-coated  $\text{Fe}_3\text{O}_4$  nanoparticles and 1.77 mmol/L  $\text{HAuCl}_4$  solution for three-time addition with an interval of 1 h. The aging time was set as 5 h.

### 3.2. Characterization

In optimized synthetic conditions, the GoldMag NPs were obtained and characterized. The TEM images show that citric acid-coated  $\text{Fe}_3\text{O}_4$  nanoparticles had an average size of 10 nm (Fig. 6a). Being darker than citric acid modified  $\text{Fe}_3\text{O}_4$  nanoparticles, the image of GoldMag NPs (Fig. 6b) displayed a spherical morphology with diameters of 10–30 nm. We employed the obtained GoldMag NPs to sonicate for 5–10 min and then separated magnetically to discard the supernatant for several times, eventually re-dispersed them in water to measure high-resolution TEM. As shown in Fig. 6c, as labeled, the spacing of 0.235 nm corresponded to the (111) reflection of the Au cubic phase, whereas the lattices of the spacing 0.253, 0.298, 0.482 nm corresponded with the (311), (220), (111) reflection of the  $\text{Fe}_3\text{O}_4$  cubic inverse spinel phase, respectively. In fact, the lattices showing the material of Au and the substance of  $\text{Fe}_3\text{O}_4$  in high resolution imaging were consistent with the XRD observation. Meanwhile, the selected area electron diffraction (SAED) patterns revealed that they were well crystallized (inserted in Fig. 6c). More importantly, these re-dispersed GoldMag NPs exhibited wine-red. When subsequently put on the side of a magnetic buckle for 5 min, the NPs quickly became colorless as shown in Fig. 6d and exhibited a good magnetic responsiveness. When we mixed the citric acid-coated  $\text{Fe}_3\text{O}_4$  and colloidal gold mechanically and separated magnetically for 5 min, we found that the color of the solution was the same as

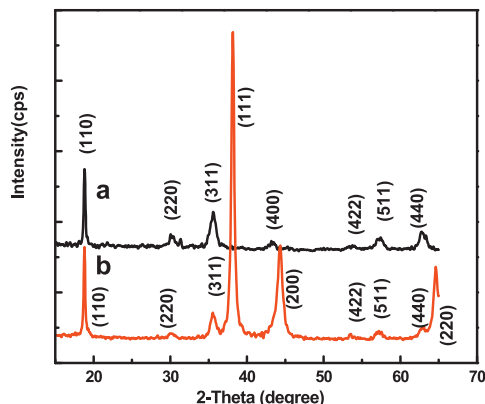


Fig. 8. X-ray diffraction patterns (XRD) for citric acid-coated  $\text{Fe}_3\text{O}_4$  (a) and GoldMag NPs (b).

that of colloidal gold (Fig. 6e). This procedure proved that the new GoldMag NPs were not simply mixed together.

Furthermore, the surface compositions of elements such as Fe and Au in GoldMag NPs were determined by X-ray photoelectron spectroscopy (XPS). Fig. 7a shows two intense peaks with the binding energies of 710.68 eV and 725.18 eV which were assigned to Fe (2p 3/2) and Fe (2p 1/2), respectively. It was typical characteristics of the  $\text{Fe}_3\text{O}_4$  structure which the two peaks including  $\text{Fe}^{2+}$  (of FeO) and  $\text{Fe}^{3+}$  (of  $\text{Fe}_2\text{O}_3$ ) peaks [29,30]. The broad peak at 718.68 eV corresponded to  $\text{Fe}^{3+}$ . The Fe (2p3/2) peak shifted slightly from 711.2 to 710.68 eV due to the formation of Au nanoparticles, indicating a strong electronic interaction between Au and  $\text{Fe}_3\text{O}_4$  [29,30]. It can be seen from Fig. 7b that the Au 4f spectrum was divided into two spin-orbit components. The peaks at 83.78 eV and 87.38 eV corresponded to  $\text{Au}^0$  4f7/2 and  $\text{Au}^0$  4f5/2, respectively, which were consistent with metallic gold [30], suggesting that GoldMag nano hybrids were synthesized successfully.

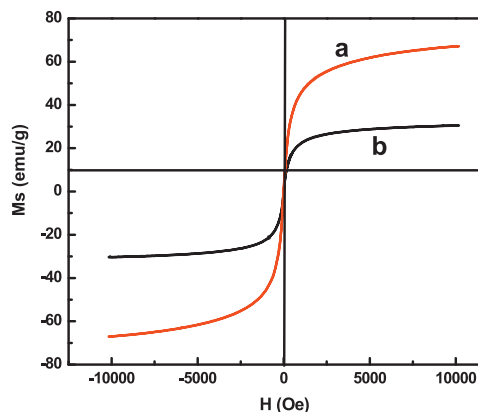


Fig. 9. Magnetic hysteresis at 300 K for citric acid-coated  $\text{Fe}_3\text{O}_4$  (a) and GoldMag NPs (b).

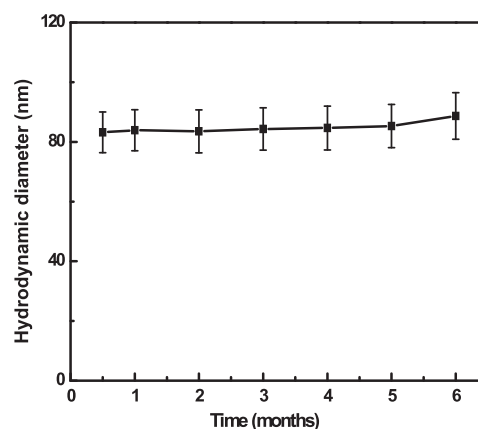
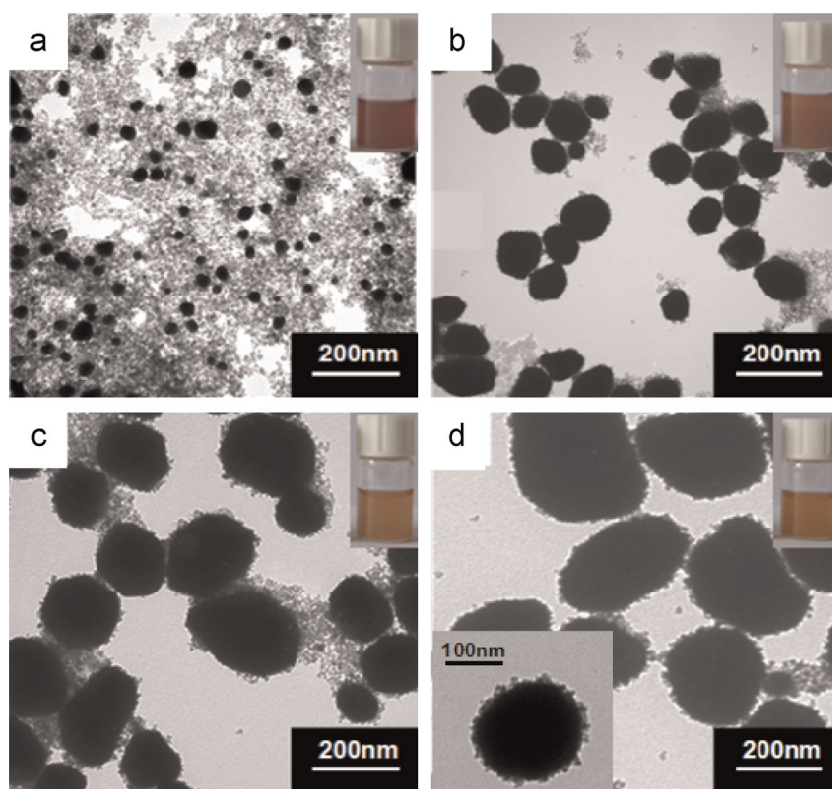


Fig. 10. Change of hydrodynamic diameter of GoldMag NPs over time.

Table 1  
Amount of reactants added for different size of GoldMag NPs.

Items	Sodium citrate (mol/L)	Citric acid-coated $\text{Fe}_3\text{O}_4$ particles (mg/L)	$\text{HAuCl}_4$ (mmol/L)
a	0.0622	40	3.54
b	0.0933	60	5.31
c	0.1244	80	7.08
d	0.1555	100	8.85



**Fig. 11.** TEM micrographs of GoldMag NPs as the reactant concentration increased in turn (a)–(d). The inset shows the pictures of corresponding GoldMag NPs dispersed in water. The inset image of TEM was much dilute GoldMag NPs as sample which was sonicated for 5–10 min and then separated magnetically to discard the supernatant for several times eventually re-dispersed in water.

The synthesized citric acid-coated  $\text{Fe}_3\text{O}_4$  nanoparticles and GoldMag NPs were compared in the XRD spectra (Fig. 8). All reflections corresponded to  $\text{Fe}_3\text{O}_4$  (JCPDS card No.79-0418). As labeled in Fig. 8b, the peaks at  $38.2^\circ$ ,  $44.4^\circ$  and  $64.58^\circ$  were assigned to the Au position of (111), (200), (220), which were located in the positions of the corresponding materials (JCPDS card No: 04-0784). The absence of diffraction peaks from magnetite had also been observed, such as  $2\theta=44.28^\circ$ . This was likely due to the heavy atom effect from Au nanoparticles as a result of interaction with citric acid-coated  $\text{Fe}_3\text{O}_4$  [31]. The XRD patterns with the diffraction peaks of both gold and  $\text{Fe}_3\text{O}_4$  validated that a composite structure of GoldMag NPs was successfully synthesized.

Magnetic properties of citric acid-coated  $\text{Fe}_3\text{O}_4$  and GoldMag NPs were also demonstrated by VSM, the magnetization loops are shown in Fig. 9. No coercivity or remanence existing at 300 K indicated the superparamagnetic behaviors of the two nanoparticles. The saturation magnetization values of citric acid-coated  $\text{Fe}_3\text{O}_4$  and GoldMag NPs were 67 and 30.2 emu/g, respectively. This showed a significant decrease for GoldMag NPs, which may be due to the diamagnetic contribution of the Au nanoparticles in the hybrid particles. Though the magnetic strength of GoldMag NPs decreased, it was still strong enough to allow the separation of GoldMag NPs by a magnet in 5 min (Fig. 6d). The inductively coupled plasma atomic emission spectroscopy (ICP-AES) analysis revealed that the mass contents of Fe and Au in GoldMag NPs were 31.6% and 47.9%, respectively.

We further tested the hydrodynamic diameter of GoldMag NPs that changed along with the storage time. As shown in Fig. 10, when stored for one month, three month, five month, the corresponding hydrodynamic diameter of GoldMag NPs was  $83.91 \pm 6.9$ ,  $84.31 \pm 7.1$ ,  $85.32 \pm 7.2$  nm, respectively. This data suggests that there are no significant differences in hydrodynamic diameter of GoldMag NPs as the storage time extends. So far, we

have just studied the storage time of GoldMag NPs up to six months. Maybe, it can maintain a longer time without significant agglomeration.

### 3.3. The controllable preparation of GoldMag NPs with different size

With the fixed ratio of reactants, we found that the size of GoldMag NPs could be effectively controlled in a wide range by adjusting the concentration of reactants. Morphologies of GoldMag NPs with the reactant concentration of 2–5 times compared with the optimized synthetic conditions are shown in Table 1. The size of GoldMag NPs ranged from 25 to 300 nm as the concentration of reactants increased as shown in Fig. 11. The colors of GoldMag NPs changed from wine-red to yellow. This scenario was also observed in optimization of  $\text{HAuCl}_4$  concentration, suggesting that both the amount and concentration of  $\text{HAuCl}_4$  solution strongly affected the sizes of GoldMag NPs. The large obtained GoldMag NPs was equally sonicated for 5–10 min and subsequently separated magnetically to discard the supernatant for several times then re-dispersed in water, at last we used the much dilute samples to measure transmission scanning electron microscope (inserted in Fig. 11d). Similar phenomena were found in TEM measurements that  $\text{Fe}_3\text{O}_4$  nanoparticles were bounded on the surface of GoldMag NPs.

## 4. Conclusion

In conclusion, we have demonstrated a novel and easy route for the fabrication of GoldMag NPs with controlled size, high dispersion, and good reproducibility. The obtained particles were characterized by UV-vis, DLS, XPS, XRD, ICP-AES and TEM. The results revealed that the GoldMag NPs were well dispersed in water with

good superparamagnetism and good magnetic responsiveness at room temperature. The average particle diameter of GoldMag NPs could be controlled from 25 to 300 nm by varying the concentration of reactants. Because of their dual advantages of Au and Fe<sub>3</sub>O<sub>4</sub> nanoparticles, GoldMag NPs with various sizes are expected to have many potential applications, such as catalysis, target delivery and protein purification.

## Acknowledgments

This work was supported by grants from the Key National Science and Technology Projects on “Key New Drug Creation and Manufacturing” (No. 2012ZX09506001), the National Natural Science Fund (No. 21303136) and Natural Science Basic Research Plan in Shaanxi Province of China (No. 2012JQ4026).

## References

- [1] M. Kuhara, H. Takeyama, T. Tanaka, T. Matsunaga, Magnetic cell separation using antibody binding with protein expressed on bacterial magnetic particles, *Anal. Chem.* 76 (2004) 6207–6213.
- [2] T.T. Hien Pham, C. Cao, S.J. Sim, Application of citrate-stabilized gold-coated ferric oxide composite nanoparticles for biological separations, *J. Magn. Magn. Mater.* 320 (2008) 2049–2055.
- [3] T. Kinoshita, S. Seino, Y. Mizukoshi, Y. Otome, T. Nakagawa, K. Okitsu, T. A. Yamamoto, Magnetic separation of amino acids by gold/iron-oxide composite nanoparticles synthesized by gamma-ray irradiation, *J. Magn. Magn. Mater.* 293 (2005) 106–110.
- [4] S. Guo, D. Li, L. Zhang, J. Li, E. Wang, Monodisperse mesoporous superparamagnetic single-crystal magnetite nanoparticles for drug delivery, *Biomaterials* 30 (2009) 1881–1889.
- [5] Y. Liang, J.L. Gong, Y. Huang, Y. Zheng, J.H. Jiang, G.L. Shen, R.Q. Yu, Biocompatible core-shell nanoparticle-based surface-enhanced Raman scattering probes for detection of DNA related to HIV gene using silica-coated magnetic nanoparticles as separation tools, *Talanta* 72 (2007) 443–449.
- [6] J. Kim, S. Park, J.E. Lee, S.M. Jin, J.H. Lee, I.S. Lee, I. Yang, J.S. Kim, S.K. Kim, M. H. Cho, T. Hyeon, Designed fabrication of multifunctional magnetic gold nanoshells and their application to magnetic resonance imaging and photothermal therapy, *Angew. Chem. Int. Ed. Eng.* 45 (2006) 7754–7758.
- [7] K. Kamei, Y. Mukai, H. Kojima, T. Yoshikawa, M. Yoshikawa, G. Kiyohara, T. A. Yamamoto, Y. Yoshioka, N. Okada, S. Seino, S. Nakagawa, Direct cell entry of gold/iron-oxide magnetic nanoparticles in adenovirus mediated gene delivery, *Biomaterials* 30 (2009) 1809–1814.
- [8] T. Zhang, W. Wang, D. Zhang, X. Zhang, Y. Ma, Y. Zhou, L. Qi, Biotemplated synthesis of gold nanoparticle–bacteria cellulose nanofiber nanocomposites and their application in biosensing, *Adv. Funct. Mater.* 20 (2010) 1152–1160.
- [9] T.T. Baby, S. Ramaprabhu, SiO<sub>2</sub> coated Fe<sub>3</sub>O<sub>4</sub> magnetic nanoparticle dispersed multiwalled carbon nanotubes based amperometric glucose biosensor, *Talanta* 80 (2010) 2016–2022.
- [10] F.H. Chen, Q.T. Chen, S.M. Fang, Y.A. Sun, Z.J. Chen, G. Xie, Y.P. Du, Multifunctional nanocomposites constructed from Fe<sub>3</sub>O<sub>4</sub>-Au nanoparticle cores and a porous silica shell in the solution phase, *Dalton Trans.* 40 (2011) 10857–10864.
- [11] Z. Gan, A. Zhao, M. Zhang, W. Tao, H. Guo, Q. Gao, R. Mao, E. Liu, Controlled synthesis of Au-loaded Fe<sub>3</sub>O<sub>4</sub>@C composite microspheres with superior SERS detection and catalytic degradation abilities for organic dyes, *Dalton Trans. (Camb., Engl.: 2003)*, 42, 8597–8605.
- [12] K.C. Grabar, R.G. Freeman, M.B. Hommer, M.J. Natan, Preparation and Characterization of Au Colloid Monolayers, *Anal. Chem.* 67 (1995) 735–743.
- [13] X. Zhao, Y. Cai, T. Wang, Y. Shi, G. Jiang, Preparation of alkanethiolate-functionalized core/shell Fe<sub>3</sub>O<sub>4</sub>@Au nanoparticles and its interaction with several typical target molecules, *Anal. Chem.* 80 (2008) 9091–9096.
- [14] S. Goergen, C. Yin, M. Yang, B. Lee, S. Lee, C. Wang, P. Wu, M.B. Boucher, G. Kwon, S. Seifert, R.E. Winans, S. Vajda, M. Flytzani-Stephanopoulos, Structure sensitivity of oxidative dehydrogenation of cyclohexane over FeO<sub>x</sub> and Au/Fe<sub>3</sub>O<sub>4</sub> nanocrystals, *ACS Catal.* 3 (2013) 529–539.
- [15] G.K. Kouassi, J. Irudayaraj, Magnetic and gold-coated magnetic nanoparticles as a DNA sensor, *Anal. Chem.* 78 (2006) 3234–3241.
- [16] T. Kinoshita, S. Seino, K. Okitsu, T. Nakayama, T. Nakagawa, T.A. Yamamoto, Magnetic evaluation of nanostructure of gold–iron composite particles synthesized by a reverse micelle method, *J. Alloys Compd.* 359 (2003) 46–50.
- [17] J.L. Lyon, D.A. Fleming, M.B. Stone, P. Schiffer, M.E. Williams, Synthesis of Fe oxide core/au shell nanoparticles by iterative hydroxylamine seeding, *Nano Lett.* 4 (2004) 719–723.
- [18] Y. Liu, T. Han, C. Chen, N. Bao, C.-M. Yu, H.-Y. Gu, A novel platform of hemoglobin on core–shell structurally Fe<sub>3</sub>O<sub>4</sub>@Au nanoparticles and its direct electrochemistry, *Electrochim. Acta* 56 (2011) 3238–3247.
- [19] H. Zhou, J. Lee, T.J. Park, S.J. Lee, J.Y. Park, J. Lee, DNA Ultrasensitive monitoring by Au–Fe<sub>3</sub>O<sub>4</sub> nanocomplex, *Sens. Actuators B: Chem.* 163 (2012) 224–232.
- [20] F. Mohammad, G. Balaji, A. Weber, R.M. Uppu, C.S. Kumar, Influence of Gold Nanoshell on Hyperthermia of Super Paramagnetic Iron Oxide Nanoparticles (SPIONs), *J. Phys. Chem. C: Nanomater. Interfaces* 114 (2010) 19194–19201.
- [21] H. Liu, P. Hou, W. Zhang, J. Wu, Synthesis of monosized core–shell Fe<sub>3</sub>O<sub>4</sub>/Au multifunctional nanoparticles by PVP-assisted nanoemulsion process, *Colloids Surfaces A: Physicochem. Eng. Asp.* 356 (2010) 21–27.
- [22] P. de la Presa, M. Multigner, M.P. Morales, T. Rueda, E. Fernández-Pinel, A. Hernando, Synthesis and characterization of FePt/Au core-shell nanoparticles, *J. Magn. Magn. Mater.* 316 (2007) e753–e755.
- [23] Y. Wu, T. Zhang, Z. Zheng, X. Ding, Y. Peng, A facile approach to Fe<sub>3</sub>O<sub>4</sub>@Au nanoparticles with magnetic recyclable catalytic properties, *Mater. Res. Bull.* 45 (2010) 513–517.
- [24] Z. Xu, Y. Hou, S. Sun, Magnetic core/shell Fe<sub>3</sub>O<sub>4</sub>/Au and Fe<sub>3</sub>O<sub>4</sub>/Au/Ag nanoparticles with tunable plasmonic properties, *J. Am. Chem. Soc.* 129 (2007) 8698–8699.
- [25] W. Hui, F. Shi, K. Yan, M. Peng, X. Cheng, Y. Luo, X. Chen, V.A. Roy, Y. Cui, Z. Wang, Fe<sub>3</sub>O<sub>4</sub>/Au/Fe<sub>3</sub>O<sub>4</sub> nanoflowers exhibiting tunable saturation magnetization and enhanced bioconjugation, *Nanoscale* 4 (2012) 747–751.
- [26] T. Goetze, C. Gansau, N. Buske, M. Roeder, P. Görnert, M. Bahr, Biocompatible magnetic core/shell nanoparticles, *J. Magn. Magn. Mater.* 252 (2002) 399–402.
- [27] J.D. Qiu, M. Xiong, R.P. Liang, H.P. Peng, F. Liu, Synthesis and characterization of ferrocene modified Fe<sub>3</sub>O<sub>4</sub>@Au magnetic nanoparticles and its application, *Biosens. Bioelectron.* 24 (2009) 2649–2653.
- [28] G. Frens, controlled nucleation for the regulation of the particle size in monodisperse gold suspensions, *Nat. Phys. Sci.* 241 (1973) 20–22.
- [29] Y.P. Wu, T. Zhang, Z.H. Zheng, X.B. Ding, Y.X. Peng, A facile approach to Fe<sub>3</sub>O<sub>4</sub>@Au nanoparticles with magnetic recyclable catalytic properties, *Mater. Res. Bull.* 45 (2010) 513–517.
- [30] H. Zhang, Y. Sun, J. Wang, J. Zhang, H.Q. Zhang, H. Zhou, D.Q. Song, Preparation and application of novel nanocomposites of magnetic-Au nanorod in SPR biosensor, *Biosens. Bioelectron.* 34 (2012) 137–143.
- [31] H. Maleki, A. Simchi, M. Imani, B.F.O. Costa, Size-controlled synthesis of superparamagnetic iron oxide nanoparticles and their surface coating by gold for biomedical applications, *J. Magn. Magn. Mater.* 324 (2012) 3997–4005.